

PML ENHANCED WITH A SELF-ADAPTIVE GOAL-ORIENTED *hp*-FINITE ELEMENT METHOD: SIMULATION OF THROUGH-CASING BOREHOLE RESISTIVITY MEASUREMENTS*

D. PARDO[†], L. DEMKOWICZ[‡], C. TORRES-VERDÍN[†], AND C. MICHLER[‡]

Abstract. We describe the application of a perfectly matched layer (PML) combined with a self-adaptive goal-oriented *hp*-finite element (FE) method to the simulation of borehole resistivity measurements. The adaptive refinements and fast convergence of the self-adaptive *hp*-FE method enhance the performance of the PML, thereby enabling the accurate and efficient truncation of the computational domain in open-domain problems. We apply this method to the simulation of axisymmetric through-casing resistivity measurements acquired in a borehole environment that are typically used for the assessment of rock formation properties. Our numerical results confirm the accuracy and efficiency of our method and provide evidence of highly accurate and reliable simulations of borehole logging measurements in the presence of a conductive steel casing and material contrast of fourteen orders of magnitude in electrical conductivity. Moreover, the combination of adaptivity and PML enables us to significantly reduce the size of the computational domain with substantial savings in computer time and memory.

Key words. *hp*-finite elements, perfectly matched layer (PML), exponential convergence, goal-oriented adaptivity, through-casing resistivity measurements

AMS subject classifications. 65M60, 78A45, 86A25

DOI. 10.1137/070689796

1. Introduction. In 1994, Berenger [3] introduced the concept of a perfectly matched layer (PML) for exterior electromagnetic problems to reduce reflections from the boundary of a truncated computational domain. During the same year, the concept of PML was recognized as complex-coordinate stretching of Maxwell’s equations by Chew and Weedon [5], which essentially means that the PML constitutes an analytic continuation of the governing equations into the complex plane; see also [24]. More recent contributions summarizing the mathematical developments and insight into PMLs can be found in [11, 23].

Let us briefly review the main idea of the PML and the difficulties pertaining to its implementation. Within the PML, both propagating and evanescent waves are transformed into evanescent waves with fast exponential decay. Thus, on the outer boundary of the PML, waves are highly attenuated in magnitude such that reflections due to an ad hoc boundary condition (BC) (for example, a homogeneous Dirichlet boundary condition) become negligible. Since the exponential decay of the waves within the PML can be made arbitrarily large, reflections from the PML can be made

*Received by the editors April 27, 2007; accepted for publication (in revised form) February 11, 2008; published electronically DATE. This work was financially supported by Baker Atlas and The University of Texas at Austin’s *Joint Industry Research Consortium on Formation Evaluation* sponsored by Aramco, Baker Atlas, BP, British Gas, Chevron, ConocoPhillips, ENI E&P, ExxonMobil, Halliburton, Marathon, Mexican Institute for Petroleum, Hydro, Occidental Petroleum, Petrobras, Schlumberger, Shell E&P, Statoil, TOTAL, and Weatherford International Ltd.

<http://www.siam.org/journals/sisc/x-x/68979.html>

[†]Department of Petroleum and Geosystems Engineering, University of Texas at Austin, Austin, TX 78712 (dzubiaur@gmail.com, cverdin@uts.cc.utexas.edu).

[‡]ICES, University of Texas at Austin, Austin, TX 78712 (leszek@ices.utexas.edu, c.michler@ices.utexas.edu). The work of the fourth author was supported by The Netherlands Organization for Scientific Research (NWO) and the ICES Postdoctoral Fellowship Program of the Institute for Computational Engineering and Sciences (ICES) at The University of Texas at Austin.

arbitrarily small. However, the rapid decay of the solution in the PML produces a “boundary layer.” Note that the resolution of such PML-induced boundary layers is crucial for the accuracy of the solution. Failing to ensure a sufficiently fine discretization in the PML typically results in spurious reflections that contaminate the solution in the entire computational domain.

Conventional discretization methods face a trade-off between using a highly attenuating PML that minimizes reflections and a PML with low attenuation that is typically easier to resolve. The more a wave is attenuated within the PML, the smaller the reflections from the truncated domain boundary, provided that the discretization can accurately resolve the rapidly changing solution in the PML. On the other hand, the more the solution is attenuated in the PML, the stronger the resulting gradients and, hence, the more difficult it is for conventional discretization methods to provide adequate resolution.

We improve the performance of the PML by combining it with a numerical method that is capable of accurately resolving strong boundary layers; see [12] for some fundamental work on this subject in the context of acoustics, elasticity, and electromagnetics. This numerical approach is based on a self-adaptive goal-oriented *hp*-finite element (FE) method that automatically, i.e., without any user interaction, constructs an accurate approximation of boundary layers with relatively few unknowns. The use of this methodology renders the design of sophisticated PMLs unnecessary. We simply select *any* PML that provides sufficiently high attenuation to eliminate reflections from the boundary; then, the self-adaptive algorithm automatically produces a grid that accurately resolves the PML-induced boundary layer. Therefore, no tuning of the PML is required to eliminate the reflections.

In this paper, we apply the PML technique combined with the self-adaptive goal-oriented *hp*-FE method to problems arising in electromagnetic logging; see [17, 18] for details and validation of the adaptive method. To this end, we investigate different PMLs (including discontinuous PMLs) to simulate challenging axisymmetric through-casing resistivity measurements in a borehole environment. In such a problem, currents propagate long distances through steel casing. To avoid the use of large computational domains, we employ the Maxwellian anisotropic PML formulation in cylindrical coordinates described in [25]. Thus, we significantly reduce the size of the computational domain, thereby eliminating unnecessarily elongated elements. It is important to note that the discretization in the PML needs to be highly accurate to avoid reflections from materials with a conductivity contrast as high as fourteen orders of magnitude.

The main challenges in the simulation of through-casing resistivity measurements pertain to high contrasts in the material properties, strong singularities, and large dynamic ranges of the solution (of up to twelve orders of magnitude for the case considered). Our main objective in these simulations is to determine the first vertical difference of electric current at two closely placed receiving coils, as we move the logging instrument in the vertical direction along the axis of the borehole. This objective function, also referred to as quantity of interest, can be used to determine the conductivity of the rock formation behind casing and thus to characterize the rock formation; see [10, 16, 20, 26, 27] for details of through-casing resistivity measurements.

The remaining sections of this paper are organized as follows: In section 2, we describe the variational formulation for axisymmetric problems and construct the PML. In section 3, we present the self-adaptive goal-oriented *hp*-FE method. In section 4, we describe the through-casing resistivity problem and present numerical results

that confirm that the PML combined with the self-adaptive hp -FE method enables a considerable reduction of the size of the computational domain without compromising the accuracy of the solution. We also demonstrate that, in combination with the PML, adaptivity in both element size h and polynomial approximation order p is necessary to ensure accuracy and efficiency of the simulations, since h -adaptivity alone turns out to be insufficient for that purpose. Finally, in section 5, we summarize the conclusions stemming from our work.

2. Maxwell's equations and PML formulation. Using cylindrical coordinates (ρ, ϕ, z) , the variational formulation of Maxwell's equations in terms of the azimuthal component of the magnetic field H_ϕ for axisymmetric problems is given by (see [14] for a detailed derivation)

$$(2.1) \quad \left\{ \begin{array}{l} \text{Find } H_\phi \in H_{\phi, \Gamma} + \tilde{H}_\Gamma^1(\Omega) \text{ such that} \\ \int_\Omega [(\bar{\sigma}_{\rho, z} + j\omega\bar{\epsilon}_{\rho, z})^{-1} \nabla \times \mathbf{H}_\phi] \cdot (\nabla \times \bar{\mathbf{F}}_\phi) dV + j\omega \int_\Omega (\bar{\boldsymbol{\mu}}_\phi \mathbf{H}_\phi) \cdot \bar{\mathbf{F}}_\phi dV \\ = - \int_\Omega M_\phi^{imp} \bar{F}_\phi dV \quad \forall F_\phi \in \tilde{H}_\Gamma^1(\Omega), \end{array} \right.$$

where $\mathbf{H}_{\phi, \Gamma}$ is a lift (in our case, $\mathbf{H}_{\phi, \Gamma} = 0$) of the essential boundary condition data,

$$\tilde{H}_\Gamma^1(\Omega) = \{F_\phi : \mathbf{F}_\phi = (0, F_\phi, 0) \in H_\Gamma(\mathbf{curl}; \Omega)\} = \left\{ F_\phi \in L^2(\Omega) : \frac{1}{\rho} F_\phi + \frac{\partial F_\phi}{\partial \rho} \in L^2(\Omega), \frac{\partial F_\phi}{\partial z} \in L^2(\Omega), F_\phi|_\Gamma = 0 \right\},$$

$F_\phi \in \tilde{H}_\Gamma^1(\Omega)$ is an arbitrary test function, \bar{F}_ϕ is the complex conjugate of F_ϕ , $\Gamma = \partial\Omega$ is the boundary of domain Ω , $\bar{\sigma}_{\rho, z}$, $\bar{\epsilon}_{\rho, z}$, are the meridian components of the electrical conductivity and dielectric permittivity of the medium, respectively, $\bar{\boldsymbol{\mu}}_\phi$ is the azimuthal component of the magnetic permeability of the medium, and M_ϕ^{imp} is the azimuthal component of a prescribed impressed magnetic current density.

We model source toroid antennas by prescribing an impressed volume magnetic current M_ϕ^{imp} on a toroidal coil equal to that induced by an electric excitation with a vertical electric dipole (VED)—also known as Hertzian dipole—of current equal to $(\sigma + j\omega\epsilon)$ Amperes. Thus, the magnetic moment of the toroid is independent of its geometrical dimensions, and, in addition, simulations performed at different frequencies may be compared without the need of frequency normalization.

A variety of BCs can be imposed to truncate the computational domain. For example, it is possible to use an infinite element technique [4], a PML [3], a boundary element technique [9], or an absorbing BC [7]. For a comparison of these truncation methods, see [8]. In this paper, we impose a homogeneous Dirichlet BC ($H_\phi = 0$) on the outer boundary of the computational domain and compare it against results obtained using a PML.

Remark. The axis of symmetry is not a boundary of the original three-dimensional problem, and therefore, no boundary condition on that axis is needed to solve the problem under consideration. Nevertheless, since the formulation of problem (2.1) requires the use of space $\tilde{H}_\Gamma^1(\Omega)$ and since this space involves the weight $\frac{1}{\rho}$ that becomes singular for $\rho \rightarrow 0$, a homogeneous Dirichlet condition at the axis of symmetry ($H_\phi|_{\rho=0} = 0$) must be specified for the discrete solution. That is, we utilize the artificial condition $H_\phi = 0$ at the axis of symmetry to ensure the proper integrability for variational formulation (2.1). Therefore, the condition imposed at the axis of symmetry should

be called the *integrability condition* rather than the *boundary condition*. Note that different proper integrability conditions may be selected in this context, $H_\phi|_{\rho=0} = 0$ being the most natural one.

2.1. PML formulation. Following [25], we construct an anisotropic Maxwellian PML by considering material properties within the PML of the form

$$(2.2) \quad \bar{\sigma} = \bar{\Lambda}\sigma; \quad \bar{\epsilon} = \bar{\Lambda}\epsilon; \quad \bar{\mu} = \bar{\Lambda}\mu,$$

where σ , ϵ , and μ are the conductivity, dielectric permittivity, and magnetic permeability of the media (assuming isotropic materials), respectively,

$$(2.3) \quad \bar{\Lambda} = \begin{bmatrix} \frac{\tilde{\rho}}{\rho} \frac{s_z}{s_\rho} & 0 & 0 \\ 0 & \frac{\rho}{\tilde{\rho}} s_z s_\rho & 0 \\ 0 & 0 & \frac{\tilde{\rho}}{\rho} \frac{s_\rho}{s_z} \end{bmatrix},$$

where $\tilde{\rho} = \int_0^\rho s_\rho(\rho') d\rho'$, and, s_ρ , s_ϕ , and s_z are the so-called stretching-coordinate functions. We define these functions as

$$(2.4) \quad s_\rho = s_\phi = s_z = 1 + \psi_i - j\psi_i,$$

where $\psi_i = \psi_i(x, x_0, x_1)$ is given by

$$(2.5) \quad \psi_i(x, x_0, x_1) = \begin{cases} 0, & x < x_0 \text{ or } x > x_1, \\ g_i(x), & x \in (x_0, x_1), \end{cases}$$

and the interval (x_0, x_1) specifies the location of the PML. We consider three different PMLs by defining three different functions $g_i(x)$ according to

$$(2.6) \quad \begin{aligned} g_1(x) &= \left[2 \left(\frac{x - x_0}{x_1 - x_0} \right) \right]^{17} && \text{PML 1,} \\ g_2(x) &= 20000 \left(\frac{x - x_0}{x_1 - x_0} \right) && \text{PML 2,} \\ g_3(x) &= 10000 && \text{PML 3.} \end{aligned}$$

The main difference between the three PMLs described in (2.6) pertains to the desired degree of smoothness. While $\psi_1(x) \in C^{16}$ (sixteen continuous derivatives) is a smooth function, $\psi_2(x) \in C^0$ (continuous function) and $\psi_3(x)$ (discontinuous function) are nonsmooth functions. The use of smooth functions $\psi_i(x)$ is commonly advocated; see, for instance, [23]. In section 5, we show that this smoothness property does not provide additional advantages when the PML is enhanced with the self-adaptive goal-oriented *hp*-FE method. In general, the solution within the PML decays (asymptotically) as an exponential function of the integral of $g_i(x)$. The higher the value of $\int g_i(x)$, the more pronounced the decay of the solution. We shall assume a PML thickness of $x_1 - x_0 = 0.5m$ throughout this paper.

We note that in order to perform reliable numerical simulations in a large frequency range, it may be more adequate to consider a frequency-dependent PML such that the corresponding solution has an asymptotically frequency-independent decay. For simplicity and clarity of the results, in this paper we restrict ourselves to frequency-independent PML.

Remark. It is well known that the use of the PML typically results in a high condition number of the associated stiffness matrix, and thus, iterative solvers may face convergence difficulties; see, e.g., [22] and the references therein. However, such convergence problems can be overcome by designing adequate preconditioners that effectively improve the condition number of the preconditioned stiffness matrix and thereby accelerate the rate of convergence of the iterative solver. Design of such preconditioners constitutes an active area of research.

3. The self-adaptive goal-oriented hp -FE method. Our numerical method is designed to have the following capabilities:

- The capability to resolve PML-induced boundary layers sufficiently accurately to avoid spurious reflections.
- The capability to accurately resolve the electromagnetic (EM) method field variation resulting from the electrical conductivity contrast that occurs between the casing and the rock formation (of up to fourteen orders of magnitude).
- The capability to accurately compute the quantity of interest $L(\mathbf{H})$ —the first vertical difference of the azimuthal component of the magnetic field— which is expected to be several orders of magnitude smaller than the magnetic field itself. The total dynamic range (the ratio between the largest value of the solution and $L(\mathbf{H})$) is expected to be of the order of 10^8 – 10^{13} .

In what follows, we describe the self-adaptive goal-oriented hp -FE method that possesses all of the above capabilities.

We utilize a numerical technique that is based on an hp -FE discretization (see [6] for details), where h denotes the element size, and p is the polynomial element order (degree) of approximation. Both h and p can vary *locally* throughout the grid. The main advantage of the hp -FE method over conventional discretization methods is that it provides exponential convergence rates of the solution with respect to the number of unknowns (as well as the CPU time), independent of the number, intensity, and/or distribution of singularities in the solution. For a proof of this result we refer to [1, 2, 21].

In order to ensure an optimal distribution of element size h and polynomial order of approximation p , we utilize a self-adaptive goal-oriented hp -adaptive strategy that minimizes the error in a user-prescribed “quantity of interest” which, for the problem under consideration, is the first vertical difference of the azimuthal component of the magnetic field, $L(\mathbf{H})$. An adaptive algorithm based on minimizing a quantity of interest of the error rather than the global energy-norm is referred to as a *goal-oriented adaptive algorithm* [19]. Goal-oriented adaptivity utilizes the solutions of two related problems: the original “direct” problem and an additional “dual” or adjoint problem that is composed of the stiffness matrix used for solving the direct problem and a right-hand side term given by the user-prescribed quantity of interest. The corresponding solution of this dual problem is called the *influence* function, which can be interpreted as a generalization of Green’s function. This influence function is utilized to guide optimal refinements. The above mentioned convergence result also extends to goal-oriented adaptivity; i.e., our algorithm also delivers exponential convergence rates for the user-prescribed quantity of interest. In particular, discretization within the PML is such that it provides optimal accuracy in terms of the user-prescribed quantity of interest. We note that even if the value of the energy-norm within the PML is small, intensive refinements within the PML may be required to accurately reproduce the quantity of interest.

The automatic adaptivity is based on the following two-grid paradigm: A given (*coarse*) conforming hp mesh is first refined globally in both h and p to yield a corresponding *fine mesh*; i.e., each element is broken into four new elements in two dimensions (eight new elements in three dimensions), and the discretization order of approximation p is raised uniformly by one. Subsequently, the problem of interest is solved on the fine mesh. The next *optimal coarse mesh* is then determined as the one that maximizes the decrease of the *projection-based interpolation error* divided by the number of added unknowns. Since the mesh optimization process is based on the minimization of the interpolation error of the solution rather than the residual, the algorithm is, in principle, problem independent. A detailed description of the hp self-adaptive goal-oriented algorithm can be found in [14, 15]. For a validation of this numerical methodology, see [16, 17, 18].

4. Numerical applications.

4.1. Through-casing resistivity applications. In this subsection, we describe the simulation problem used for the numerical experiments detailed in subsection 4.2. We consider a through-casing resistivity problem that is commonly utilized to probe subsurface rock formations with electromagnetic waves.

Using cylindrical coordinates (ρ, ϕ, z) , we specify the following geometry, sources, receivers, and materials (see also the illustration in Figure 4.1):

- One 9cm radius toroidal coil with a $1\text{cm} \times 1\text{cm}$ cross-section located on the axis of symmetry and moving along the z -axis, and two receiving coils of the same dimensions located 150cm and 175cm , respectively, above the source antenna.
- Borehole: A cylinder Ω_I of radius 10cm surrounding the axis of symmetry ($\Omega_I = \{(\rho, \phi, z) : \rho \leq 10\text{cm}\}$), with resistivity $R = 0.1 \Omega \cdot m$.
- Casing: A steel casing Ω_{II} of width 1.27cm surrounding the borehole ($\Omega_{II} = \{(\rho, \phi, z) : 10\text{cm} \leq \rho \leq 11.27\text{cm}\}$), with resistivity $R = 0.000001 \Omega \cdot m = 10^{-6} \Omega \cdot m$.
- Formation material I: A subdomain Ω_{III} defined by $\Omega_{III} = \{(\rho, \phi, z) : \rho > 11.27\text{cm}, 0\text{cm} \leq z \leq 100\text{cm}\}$, with resistivity $R = 10000 \Omega \cdot m$.
- Formation material II: A subdomain Ω_{IV} defined by $\Omega_{IV} = \{(\rho, \phi, z) : \rho > 11.27\text{cm}, -50\text{cm} \leq z < 0\text{cm}\}$, with resistivity $R = 0.01 \Omega \cdot m$.
- Formation material III: A subdomain Ω_V defined by $\Omega_V = \{(\rho, \phi, z) : \rho > 11.27\text{cm}, z < -50\text{cm}, \text{ or } z > 100\text{cm}\}$, with resistivity $R = 5 \Omega \cdot m$.

The quantity of interest $L(\mathbf{H})$ for these simulations is the first difference of electric current I at the two receiving coils (l_1 and l_2) of radius $a = 9\text{cm}$ divided by the (vertical) distance Δz between the two receiving coils, i.e.,

$$(4.1) \quad L(\mathbf{H}) = \frac{I_1 - I_2}{\Delta z} = \frac{\oint_{l_1} \mathbf{H}(l) \, dl - \oint_{l_2} \mathbf{H}(l) \, dl}{\Delta z}.$$

In this paper, we consider a variation of resistivity of the casing from $10^{-10} \Omega \cdot m$ to $10^{-6} \Omega \cdot m$. We first perform simulations at a realistic operating frequency of 1 Hz , and then we study in Figure 4.10 the effects of frequency variations.

4.2. Numerical results. Below, we present the numerical simulations of the resistivity logging problem in a case well described in subsection 4.1. The transmitter coil is assumed to be located at $z = -1.65\text{m}$.

First, we study the importance of the size of the computational domain when we consider ad hoc boundary conditions—homogeneous Neumann boundary conditions

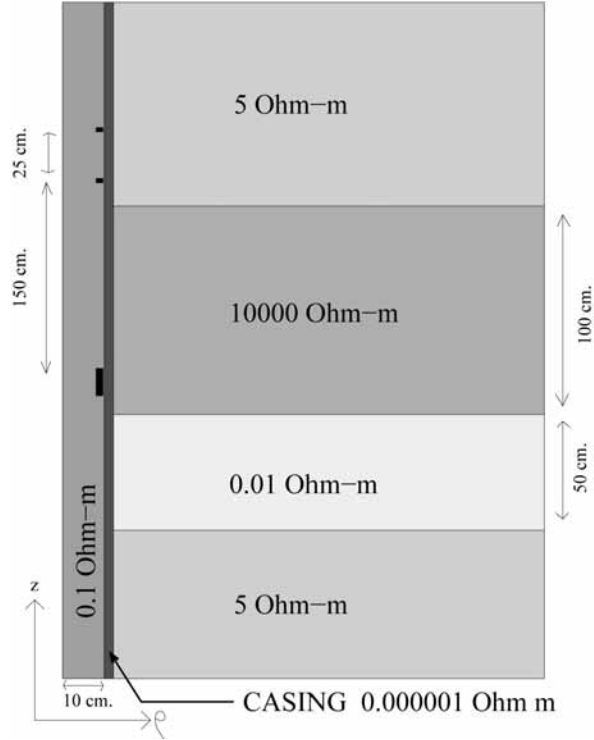


FIG. 4.1. *Two-dimensional cross-section of the geometry of a through-casing resistivity problem. Measurement instruments consist of one transmitter and two receiver coils. The model includes a conductive borehole, a metallic casing, and four layers in the formation material with varying resistivities.*

at the top and bottom of the domain, and homogeneous Dirichlet boundary conditions at the side—without a PML. In this context, we shall refer to the error due to the truncation of the computational domain as the modeling error and use the solution obtained with PML 1 ($10m \times 5m$ domain) as the reference solution. This choice of reference solutions is justified, since the selected PML strongly attenuates the solution, thereby minimizing reflections. Thus, the modeling error of the reference solution, which is due to the replacement of the almost-zero solution on the outer part of the PML by a homogeneous Dirichlet BC ($H_\phi = 0$) is negligible. Our numerical results further support this choice of reference solutions. Figures 4.2 and 4.3 display the relative error of the real and imaginary parts, respectively, of the quantity of interest given by (4.1) as a function of the vertical length of the computational domain. The horizontal length of the domain is taken to be one-fourth of the vertical length, since casing is present only in the vertical direction.

From Figures 4.2 and 4.3, we observe that in order to guarantee a modeling error below 1% we need to consider large computational domains that are several kilometers in size. In particular, for a casing resistivity equal to $10^{-6}\Omega \cdot m$, a domain with vertical length equal to $10000m$ still delivers relative errors in the imaginary part greater than 1%. This error can be attributed to the truncation of the computational

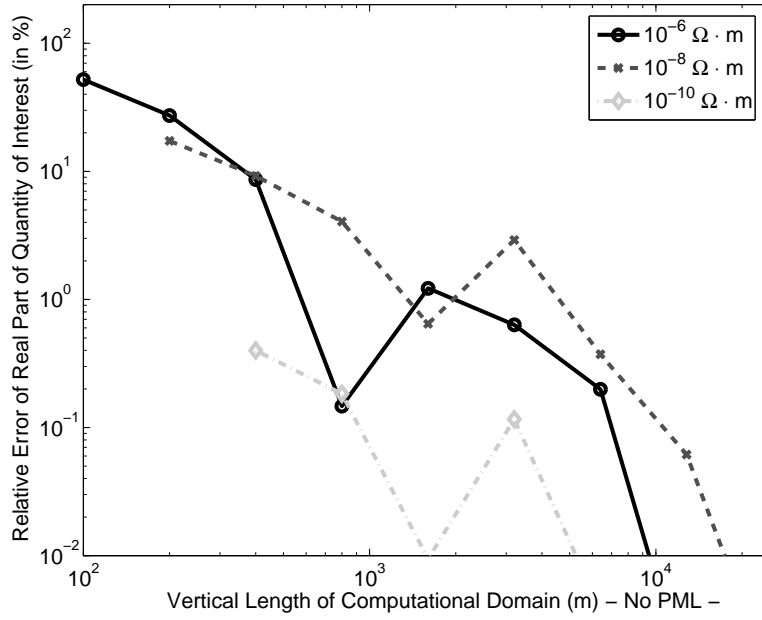


FIG. 4.2. Through-casing resistivity problem. Relative error of the real part of the quantity of interest according to (4.1) as a function of the vertical length of the computational domain. Different curves indicate different resistivities of the casing, ranging from $10^{-10} \Omega \cdot m$ to $10^{-6} \Omega \cdot m$. Results obtained with goal-oriented hp-adaptivity.

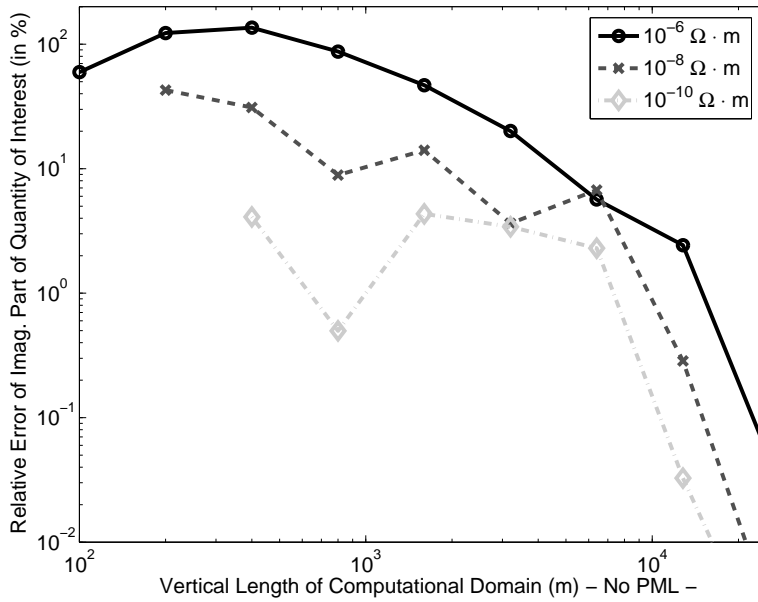


FIG. 4.3. Through-casing resistivity problem. Relative error of the imaginary part of the quantity of interest according to (4.1) as a function of the vertical length of the computational domain. Different curves indicate different resistivities of the casing, ranging from $10^{-10} \Omega \cdot m$ to $10^{-6} \Omega \cdot m$. Results obtained with goal-oriented hp-adaptivity.

domain.¹ Moreover, Figures 4.2 and 4.3 indicate a nonmonotonic behavior of the error as a function of the size of the computational domain. Although we do not have a rigorous explanation for this observation, such nonmonotonic behavior prompts a word of caution in that it renders the selection of an optimal domain size difficult. In particular, assuming a monotonic behavior based on an extrapolation of a small set of numerical results may be misleading, since it does not reflect the actual dependence of the error on the domain length and, thus, may lead to the selection of an inappropriate size of the computational domain.

Table 4.1 complements the results shown in Figures 4.2 and 4.3 by displaying the quantity of interest given by (4.1) corresponding to the three different PMLs considered in this paper. We observe that with any of the three different PMLs (and a computational domain of $5m \times 2.5m$) we obtain more accurate results than those obtained by considering a computational domain of $12800m \times 3200m$ without a PML. This result confirms the high accuracy obtained with the use of PMLs enhanced with the self-adaptive goal-oriented *hp*-FE method.

TABLE 4.1

Through-casing resistivity problem. Real and imaginary parts of the quantity of interest—given by (4.1)—as a function of the size of the computational domain and presence of a PML. Results obtained with goal-oriented hp-adaptivity.

Resistivity casing	Domain size (m)	Real part (A/m)	Imag. part (A/m)
$10^{-6} \Omega \cdot m$	PML 1 (5 x 2.5)	1.2320E-6	-8.5928E-9
$10^{-6} \Omega \cdot m$	PML 2 (5 x 2.5)	1.2320E-6	-8.5960E-9
$10^{-6} \Omega \cdot m$	PML 3 (5 x 2.5)	1.2320E-6	-8.6016E-9
$10^{-6} \Omega \cdot m$	400 x 100	1.3382E-6	-2.0264E-8
$10^{-6} \Omega \cdot m$	1600 x 400	1.2169E-6	-1.2622E-8
$10^{-6} \Omega \cdot m$	6400 x 1600	1.2295E-6	-8.1076E-9
$10^{-6} \Omega \cdot m$	12800 x 3200	1.2320E-6	-8.3840E-9
$10^{-6} \Omega \cdot m$	25600 x 6400	1.2320E-6	-8.5968E-9
$10^{-8} \Omega \cdot m$	PML 1 (5 x 2.5)	1.7188E-10	-2.0959E-11
$10^{-8} \Omega \cdot m$	PML 2 (5 x 2.5)	1.7188E-10	-2.0959E-11
$10^{-8} \Omega \cdot m$	PML 3 (5 x 2.5)	1.7188E-10	-2.0957E-11
$10^{-8} \Omega \cdot m$	400 x 100	1.8772E-10	-1.4463E-11
$10^{-8} \Omega \cdot m$	1600 x 400	1.7077E-10	-2.3905E-11
$10^{-8} \Omega \cdot m$	6400 x 1600	1.7124E-10	-1.9548E-11
$10^{-8} \Omega \cdot m$	12800 x 3200	1.7120E-10	-2.0900E-11
$10^{-8} \Omega \cdot m$	25600 x 6400	1.7188E-10	-2.0960E-11
$10^{-10} \Omega \cdot m$	PML 1 (5 x 2.5)	1.4255E-13	2.2710E-15
$10^{-10} \Omega \cdot m$	PML 2 (5 x 2.5)	1.4255E-13	2.2710E-15
$10^{-10} \Omega \cdot m$	PML 3 (5 x 2.5)	1.4255E-13	2.2709E-15
$10^{-10} \Omega \cdot m$	400 x 100	1.4198E-13	2.1780E-15
$10^{-10} \Omega \cdot m$	1600 x 400	1.4256E-13	2.3695E-15
$10^{-10} \Omega \cdot m$	6400 x 1600	1.4256E-13	2.2188E-15
$10^{-10} \Omega \cdot m$	12800 x 3200	1.4255E-13	2.2703E-15
$10^{-10} \Omega \cdot m$	25600 x 6400	1.4255E-13	2.2710E-15

Next, we analyze the computational cost for PMLs combined with our adaptive al-

¹The discretization error is several orders of magnitude smaller than the modeling error. We verified this claim using an error estimator based on the solution of the problem on a globally refined (in both h and p) grid. See [13] for additional details about the error estimator.

gorithm. For each computational domain we study the behavior of the discretization error (disregarding the modeling error due to the truncation of the computational domain) as a function of the problem size (number of unknowns). Table 4.2 displays the discretization error and the corresponding number of unknowns for different computational domains. Note that these results depend on the initial grid, which is different for each computational domain (although all of them are based on geometrically graded grids). Nevertheless, the results reported in Table 4.2 provide an indication of the performance associated with each computational domain and PML. These results show a considerable reduction of the problem size (about 50%) in terms of the number of unknowns when introducing PML 2 as opposed to all other cases displayed in Table 4.2. It is noteworthy that even with the poorly designed discontinuous PML 3 we obtain results that are competitive with those of the remaining cases, since the corresponding solution is also piecewise smooth.

TABLE 4.2

Through-casing resistivity problem. Number of unknowns employed by the self-adaptive goal-oriented hp-FE method as a function of the size of the computational domain and presence of a PML.

Resistivity casing	Domain size (m)	No. unknowns ($\approx 1\%$ error)	No. unknowns ($\approx 0.01\%$ error)
$10^{-6} \Omega \cdot m$	PML 1 (5×2.5)	19541 (0.083%)	24886 (0.037%)
$10^{-6} \Omega \cdot m$	PML 2 (5×2.5)	7095 (0.29%)	13345 (0.006%)
$10^{-6} \Omega \cdot m$	PML 3 (5×2.5)	8679 (1.04%)	19640 (0.009%)
$10^{-6} \Omega \cdot m$	6400 x 1600	12327 (0.43%)	18850 (0.014%)
$10^{-6} \Omega \cdot m$	12800 x 3200	12327 (0.43%)	18850 (0.014%)
$10^{-6} \Omega \cdot m$	25600 x 6400	12099 (1.22%)	19828 (0.037%)
$10^{-8} \Omega \cdot m$	PML 1 (5×2.5)	12702 (0.214%)	27291 (0.002%)
$10^{-8} \Omega \cdot m$	PML 2 (5×2.5)	7787 (0.832%)	18115 (0.003%)
$10^{-8} \Omega \cdot m$	PML 3 (5×2.5)	10857 (0.750%)	28954 (0.083%)
$10^{-8} \Omega \cdot m$	6400 x 1600	11433 (0.262%)	20109 (0.013%)
$10^{-8} \Omega \cdot m$	12800 x 3200	14305 (1.262%)	28834 (0.012%)
$10^{-8} \Omega \cdot m$	25600 x 6400	21400 (0.384%)	32178 (0.011%)
$10^{-10} \Omega \cdot m$	PML 1 (5×2.5)	5957 (0.811%)	14497 (0.004%)
$10^{-10} \Omega \cdot m$	PML 2 (5×2.5)	4714 (1.056%)	12378 (0.004%)
$10^{-10} \Omega \cdot m$	PML 3 (5×2.5)	5942 (0.988%)	11812 (0.011%)
$10^{-10} \Omega \cdot m$	6400 x 1600	8805 (1.530%)	13786 (0.004%)
$10^{-10} \Omega \cdot m$	12800 x 3200	8545 (0.872%)	17521 (0.019%)
$10^{-10} \Omega \cdot m$	25600 x 6400	6597 (1.103%)	18245 (0.039%)

Figures 4.4 and 4.5 display the logs² corresponding to a casing resistivity equal to $10^{-6} \Omega \cdot m$ and $10^{-10} \Omega \cdot m$, respectively. We computed these logs by utilizing two different computational domains, viz. a $10m \times 5m$ domain with PML 2, and a $3200m \times 800m$ domain without a PML. Figure 4.4 shows that the computed amplitude is similar for both computational domains whereas the phase is significantly different. This behavior indicates that a large computational domain of $3200m \times 800m$ without a PML can induce a considerable phase error. In Figure 4.5, we obtain similar results when considering either of the two computational domains described above.

²A log is a plot displaying the measurement of the logging instrument as we move it in the vertical direction along the axis of the borehole.

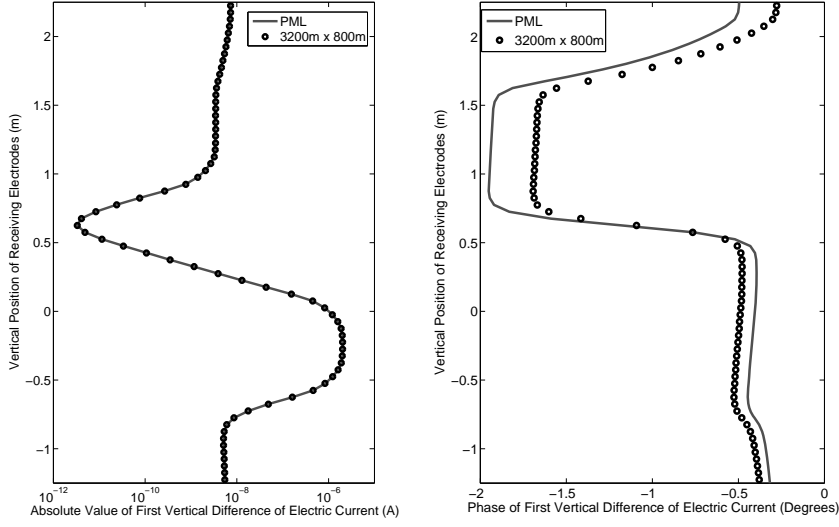


FIG. 4.4. Through-casing resistivity problem with a resistivity of casing equal to $10^{-6}\Omega \cdot m$. Amplitude (left) and phase (right) of the final log. The two curves were obtained on two different computational domains: A $10m \times 5m$ domain with PML 3, and a $3200m \times 800m$ domain without a PML. Results obtained with goal-oriented hp-adaptivity.

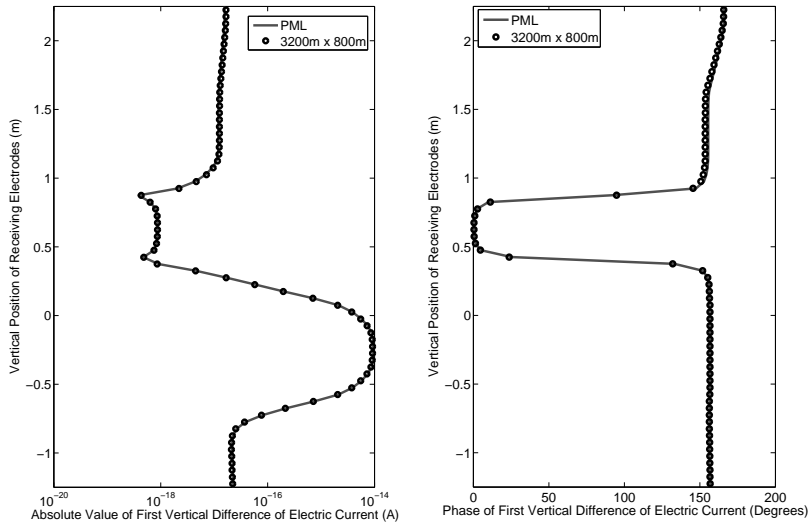


FIG. 4.5. Through-casing resistivity problem with a resistivity of casing equal to $10^{-10}\Omega \cdot m$. Amplitude (left) and phase (right) of the final log. The two curves were obtained on two different computational domains: A $10m \times 5m$ domain with PML 3, and a $3200m \times 800m$ domain without a PML. Results obtained with goal-oriented hp-adaptivity.

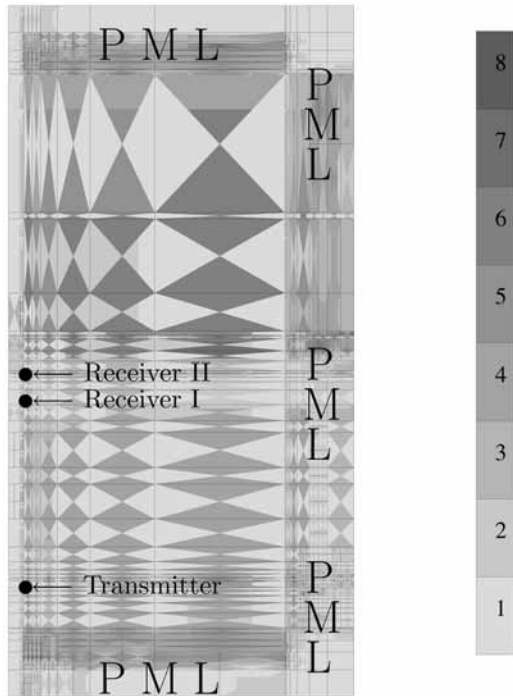


FIG. 4.6. Through-casing resistivity problem. hp -grid with 7421 unknowns delivered by the self-adaptive goal-oriented hp -FE method. Different colors indicate different polynomial orders of approximation, from 1 (light) up to 9 (dark). Size of computational domain: $5m \times 2.5m$, including a $0.5m$ thick PML.

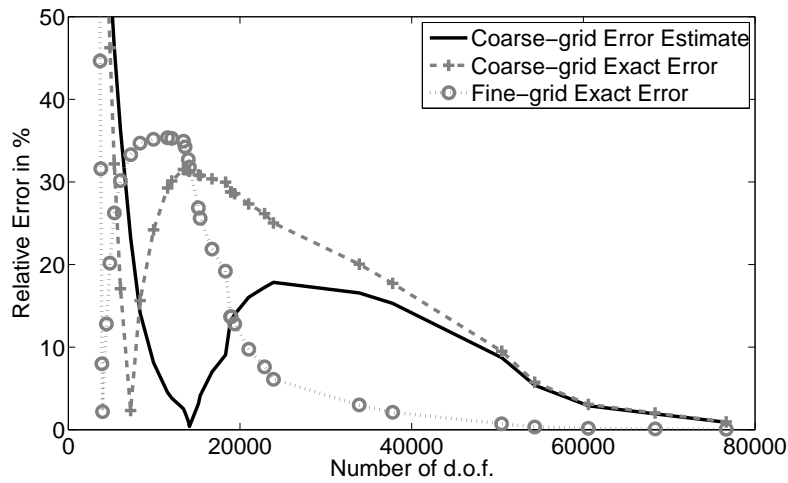


FIG. 4.7. Through-casing resistivity problem with resistivity of casing equal to $10^{-6}\Omega \cdot m$. Convergence history (number of degrees of freedom—unknowns—of the coarse grid vs. relative error of the quantity of interest in percentage) delivered by the self-adaptive goal-oriented h -FE method, with $p = 2$, combined with the PML 2 ($5m \times 2.5m$).

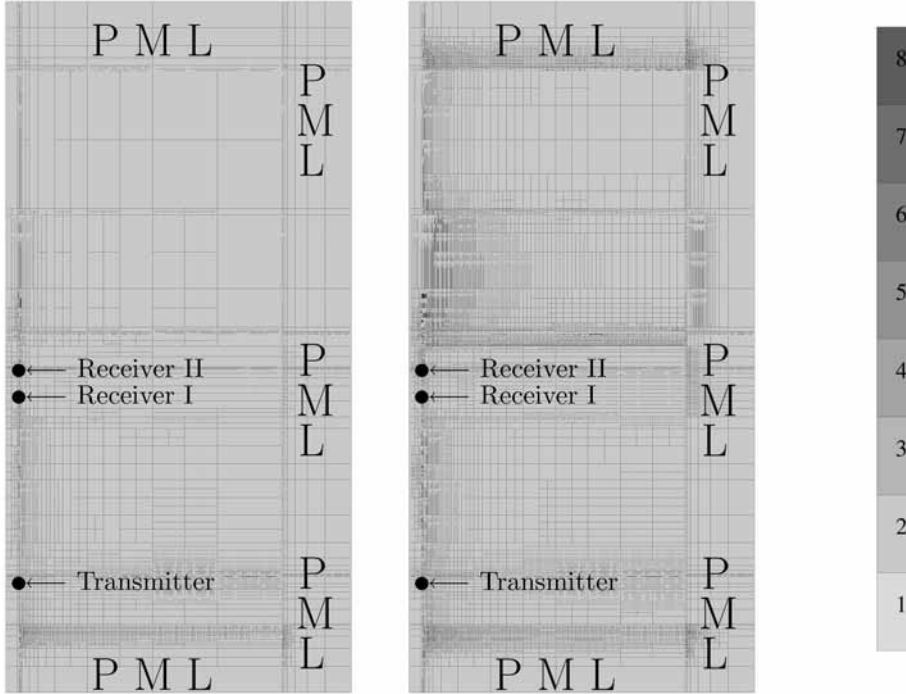


FIG. 4.8. Through-casing resistivity problem. Two h -grids (with $p = 2$) delivered by the self-adaptive goal-oriented h -FE method. Left panel: Intermediate h -grid with 14105 unknowns, delivering an error of over 30%. Right panel: Final h -grid with 76643 unknowns, delivering an error of 2%. Size of computational domain: $5m \times 2.5m$, including a $0.5m$ -thick PML 2.

We observe a large frequency shift of approximately 160 degrees in Figure 4.5 due to the presence of a highly conductive casing in a highly resistive formation, as can be physically expected. In addition, a “horn” in the amplitude ensues when compared to Figure 4.4.

An hp -grid produced by the self-adaptive goal-oriented hp -FE method with PML 2 and a casing resistivity equal to $10^{-6} \Omega \cdot m$ is displayed in Figure 4.6 for exemplification purposes. The grid contains 7421 unknowns (of which 80% are used in the PML), and it delivers a discretization error in the quantity of interest below 0.2%. Large elements of high-order approximation are effective in approximating the smooth part of the solution, while small elements of low order are more suitable for approximating abrupt spatial variations due to singularities in the solution. In the outer part of the casing, we observe more refinements than in the inner part of the casing, since it is physically known that the quantity of interest exhibits little sensitivity to the conductivity inside the borehole.

To assess the importance of refinements in both h and p , let us now consider an adaptive goal-oriented FE method with fixed polynomial order of approximation p but variable mesh size h . To guide optimal refinements for a given coarse h -grid, we utilize the globally h -refined grid, that is, the $h/2$ -grid, where, in two dimensions, all elements are divided into four new elements. We denote the globally h -refined grid as the fine grid. Then, we employ an adaptive strategy that is analogous to the one for hp -adaptivity with the only provision that the polynomial order of approximation p

remains unchanged.

Figure 4.7 displays the convergence behavior of the h -adaptive method restricted to polynomial-approximation order $p = 2$ (quadratic basis functions) and combined with a PML, where the discretization error is measured with reference to the solution that is provided by the hp -adaptive method. The results displayed in Figure 4.7 and their comparison to the results given in Table 4.2 indicate that the h -adaptive method combined with a PML is less accurate for solving the through-casing resistivity problem under consideration. This observation indicates that in the present case, a restriction of the approximation order to $p = 2$ significantly limits the efficiency of the method when compared to the hp -adaptive method. In particular, we observe that the sequence of coarse h -grids delivers for 50000 unknowns an error that is still larger than 10%. Furthermore, for any coarse grid with fewer than 15000 unknowns, the fine grid delivers large errors (above 30%) and, therefore, is unable to guide optimal refinements. To further support this observation, we display in Figure 4.8 two optimal coarse h -grids, where the first one (left panel) contains an intermediate (optimal) h -grid with 14105 unknowns. The estimated relative error (computed as the difference between the solutions obtained on the h - and $h/2$ -grids, respectively) is below 1%. However, the actual (exact) error is above 30%, since the fine grid fails to deliver an accurate reference solution. Indeed, we observe in Figure 4.8 (left panel) that the PML in the upper part of the domain is underresolved.

Let us briefly summarize our findings for h -adaptivity when restricting ourselves

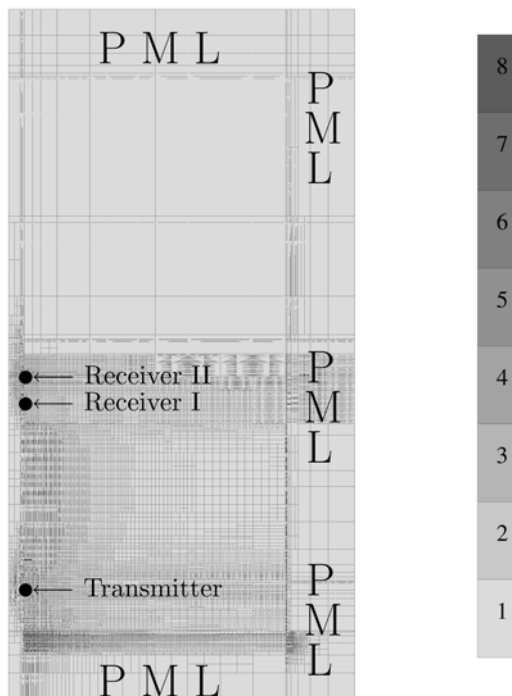


FIG. 4.9. Through-casing resistivity problem. Final h -grid with $p = 1$, containing 104834 unknowns and delivering an error over 50%. Size of computational domain: $5\text{m} \times 2.5\text{m}$, including a 0.5m -thick PML 2.

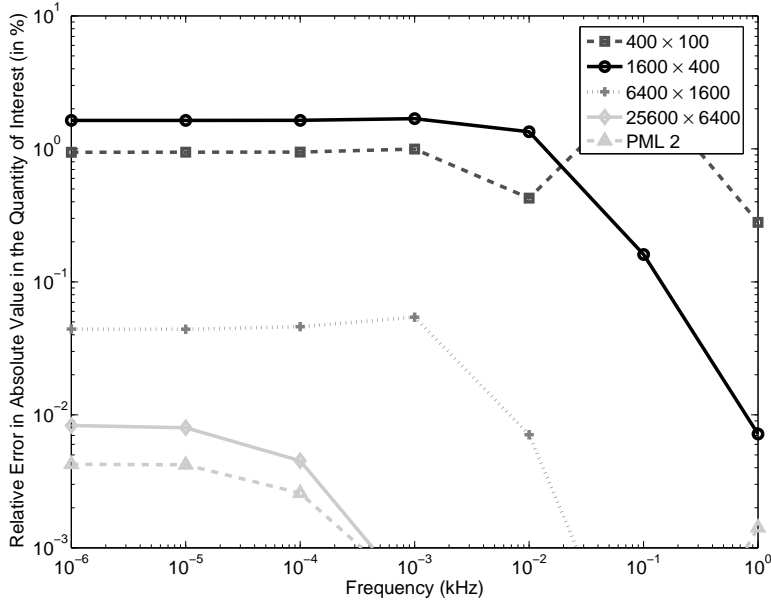


FIG. 4.10. Anisotropic through-casing resistivity problem with resistivity of casing equal to $10^{-6}\Omega \cdot m$. Relative error of the absolute value of the quantity of interest as a function of the frequency. Different curves indicate different domain sizes: $400m \times 100m$, $1600m \times 400m$, $6400m \times 1600m$, $25600m \times 6400m$, and $5m \times 2.5m$ (with PML 2). Results obtained with goal-oriented hp-adaptivity.

to linear elements ($p = 1$) that are commonly used in engineering practice. Our numerical experiments indicate that, for linear elements, an h -adapted grid with over 100000 unknowns is still not sufficiently fine to reduce the relative error in the quantity of interest below 50% for the problem under consideration. The final h -grid, displayed in Figure 4.9, contains over 100000 unknowns; however, it still exhibits a relative error in the quantity of interest over 50%. Similarly, we observe in the final h -grid that the upper part of the domain, including the PML, is underresolved.

Finally, we reconsider our original through-casing resistivity problem, and we replace the upper layer of the formation (with resistivity equal to $5\Omega \cdot m$) by an anisotropic material with horizontal resistivity equal to $1\Omega \cdot m$ and vertical resistivity equal to $5\Omega \cdot m$. In so doing, we consider a casing resistivity equal to $10^{-6}\Omega \cdot m$. Utilizing the solution obtained with PML 1 as a reference solution, we plot in Figure 4.10 the error due to truncation of the computational domain versus frequency. By employing either PML 2 or a large computational domain of size equal to $25000m \times 6400m$, we obtain a total error below 0.01%, which is the discretization error tolerance that we previously selected for this problem. When considering smaller domains, we appraise the effect of domain truncation error which may become as large as 5% for a domain of size $1600m \times 400m$. As a general trend, Figure 4.10 indicates a monotonic decrease of the error with increasing frequency (as physically expected). Note, however, that there are conspicuous exceptions to this monotonic behavior as evidenced by the simulation results shown in Figure 4.10.

5. Conclusions. We have shown that numerical reflections due to domain truncation for a layered medium with high-material contrasts are efficiently minimized with a self-adaptive goal-oriented hp -FE method in combination with a PML. Such an adaptive method is capable of delivering optimal grid refinements, and, hence, it can substantially improve the performance of PMLs.

For problems with material coefficients varying by up to ten orders of magnitude within the PML, the self-adaptive goal-oriented hp -FE method automatically constructs a grid that exhibits minimum reflections (below 0.001% relative error in the quantity of interest for a moderate number of unknowns), even when considering discontinuous PMLs. Thus, for through-casing resistivity measurements, one can reduce the size of the computational domain from, for instance, $25000m$ to $5m$ using a PML in combination with our adaptive algorithm. We have shown that this approach compromises neither the accuracy of the magnitude nor the phase of the computed logging response. Moreover, the number of unknowns that are needed to solve the problem within prescribed accuracy can be significantly reduced using a PML enhanced with adaptivity instead of a large domain without PML. Thus, we have shown that PMLs can be successfully employed not only for pure wave propagation problems with quasi-uniform materials, but also for engineering applications with high material contrast within the PML region.

In this paper, we have also shown that a PML combined with a goal-oriented FE method that is self-adaptive only in the element size h may be considerably less accurate than the corresponding hp -method and require several orders of magnitude more unknowns to achieve the same level of accuracy. This behavior indicates that adaptivity in both element size h and polynomial approximation order p is essential for the accuracy of the solution.

Finally, we have shown that PMLs combined with the self-adaptive goal-oriented hp -FE method maintain good computer performance in the presence of anisotropic materials, regardless of the frequency of operation.

REFERENCES

- [1] I. BABUSKA AND B. GUO, *Approximation properties of the h-p version of the finite element method*, Comput. Methods Appl. Mech. Engrg., 133 (1996), pp. 319–346.
- [2] I. BABUŠKA AND B. Q. GUO, *Regularity of the solution of elliptic problems with piecewise analytic data. I. Boundary value problems for linear elliptic equations of second order*, SIAM J. Math. Anal., 19 (1988), pp. 172–203.
- [3] J.-P. BERENGER, *A perfectly matched layer for the absorption of electromagnetic waves*, J. Comput. Phys., 114 (1994), pp. 185–200.
- [4] W. CECOT, W. RACHOWICZ, AND L. DEMKOWICZ, *An hp-adaptive finite element method for electromagnetics. III. A three-dimensional infinite element for Maxwell's equations*, Internat. J. Numer. Methods Engrg., 57 (2003), pp. 899–921.
- [5] W. C. CHEW AND W. H. WEEDON, *A 3D perfectly matched medium from modified Maxwell's equations with stretched coordinates*, Microwave Opt. Tech. Lett., 7 (1994), pp. 599–604.
- [6] L. DEMKOWICZ, *Computing with hp-Adaptive Finite Elements. Volume I: One and Two Dimensional Elliptic and Maxwell Problems*, Chapman and Hall, Boca Raton, FL, 2007.
- [7] B. ENGQUIST AND A. MAJDA, *Absorbing boundary conditions for the numerical simulation of waves.*, Math. Comput., 31 (1977), pp. 629–651.
- [8] I. GOMEZ-REVUELTO, L. GARCIA-CASTILLO, AND L. DEMKOWICZ, *A comparison between several mesh truncation methods for hp-adaptivity in electromagnetics*, in International Conference on Electromagnetics in Advanced Applications (ICEAA07), Torino, Italy, 2007. Invited paper to the Special Session “Numerical Methods for Solving Maxwell Equations in the Frequency Domain.”
- [9] I. GOMEZ-REVUELTO, L. E. GARCIA-CASTILLO, D. PARDO, AND L. DEMKOWICZ, *A two-dimensional self-adaptive hp finite element method for the analysis of open region problems*

- in electromagnetics*, IEEE Trans. Magnetics, 43 (2007), pp. 1337–1340.
- [10] A. A. KAUFMAN, *The electrical field in a borehole with casing*, Geophysics, 55 (1990), pp. 29–38.
- [11] M. KUZUOGLU AND R. MITTRA, *A systematic study of perfectly matched absorbers*, in *Frontiers in Electromagnetics*, D. H. Werner and R. Mittra, eds., John Wiley and Sons, New York, 2000, pp. 609–642.
- [12] C. MICHLER, L. DEMKOWICZ, J. KURTZ, AND D. PARDO, *Improving the performance of perfectly matched layers by means of hp-adaptivity*, Numer. Methods Partial Differential Equations, 23 (2007), pp. 832–858.
- [13] D. PARDO, L. DEMKOWICZ, C. TORRES-VERDIN, AND M. PASZYNSKI, *Two-dimensional high-accuracy simulation of resistivity logging-while-drilling (LWD) measurements using a self-adaptive goal-oriented hp finite element method*, SIAM J. Appl. Math., 66 (2006), pp. 2085–2106.
- [14] D. PARDO, L. DEMKOWICZ, C. TORRES-VERDIN, AND M. PASZYNSKI, *A self-adaptive goal-oriented hp adaptive finite element method with electromagnetic applications. Part II: Electrodynamics*, Comput. Methods Appl. Mech. Engrg., 196 (2007), pp. 3585–3597.
- [15] D. PARDO, L. DEMKOWICZ, C. TORRES-VERDIN, AND L. TABAROVSKY, *A goal-oriented hp adaptive finite element method with electromagnetic applications. Part I: Electrostatics*, Internat. J. Numer. Methods Engrg., 65 (2006), pp. 1269–1309.
- [16] D. PARDO, C. TORRES-VERDIN, AND L. DEMKOWICZ, *Simulation of multi-frequency borehole resistivity measurements through metal casing using a goal-oriented hp-finite element method*, IEEE Trans. Geosci. Remote Sens., 44 (2006), pp. 2125–2135.
- [17] D. PARDO, C. TORRES-VERDIN, AND L. DEMKOWICZ, *Feasibility study for two-dimensional frequency-dependent electromagnetic sensing through casing*, Geophysics, 72 (2007), pp. F111–F118.
- [18] M. PASZYNSKI, L. DEMKOWICZ, AND D. PARDO, *Verification of goal-oriented hp-adaptivity*, Comput. Math. Appl., 50 (2005), pp. 1395–1404.
- [19] S. PRUDHOMME AND J. T. ODEN, *On goal-oriented error estimation for elliptic problems: Application to the control of pointwise errors*, Comput. Methods Appl. Mech. Engrg., 176 (1999), pp. 313–331.
- [20] C. J. SCHENKEL AND H. F. MORRISON, *Electrical resistivity measurement through metal casing*, Geophysics, 59 (1994), pp. 1072–1082.
- [21] C. SCHWAB, *p- and hp-Finite Element Methods. Theory and Applications in Solid and Fluid Mechanics*, Numer. Math. Sci. Comput., The Clarendon Press, Oxford University Press, New York, 1998.
- [22] B. STUPFEL, *A study of the condition number of various finite element matrices involved in the numerical solution of Maxwell's equations*, IEEE Trans. Antennas and Propagation, 52 (2004), pp. 3048–3059.
- [23] F. TEIXEIRA AND W. CHEW, *Advances in the theory of perfectly matched layers*, in *Fast and Efficient Algorithms in Computational Electromagnetics*, W. C. Chew, J. M. Jin, E. Michielson, and J. M. Song, eds., Artech House, Boston, 2001, pp. 283–346.
- [24] F. L. TEIXEIRA AND W. C. CHEW, *PML-FDTD in cylindrical and spherical grid*, IEEE Microw. Guid. Wave Lett., 7 (1997), pp. 285–287.
- [25] F. L. TEIXEIRA AND W. C. CHEW, *Systematic derivation of anisotropic PML absorbing media in cylindrical and spherical coordinates*, IEEE Microw. Guid. Wave Lett., 7 (1997), pp. 371–373.
- [26] W. VAIL, S. MOMI, R. WOODHOUSE, M. ALBERTY, R. PEVERARO, AND J. KLEIN, *Formation resistivity measurements through metal casing*, SPWLA 34th Annual Logging Symposium, Alberta, Canada, 1993, pp. 1–21.
- [27] X. WU AND T. M. HABASHY, *Influence of steel casings on electromagnetic signals*, Geophysics, 59 (1994), pp. 378–390.